Catal Lett (2012) 142:646–654
DOI 10.1007/s10562-012-0788-2

Enhanced Photodegradation of Toxic Pollutants on Plasmonic Au–Ag–AgI/Al_2O_3 Under Visible Irradiation

Tianwei Peng · Chun Hu · Xuexiang Hu · Xuefeng Zhou · Jiuhui Qu

Received: 19 December 2011 / Accepted: 22 February 2012 / Published online: 13 March 2012

Abstract Au–Ag–AgI nanoparticles (NPs) were uniformly dispersed onto mesoporous alumina by deposition–precipitation and photoreduction at low temperature. Compared with Ag–AgI/Al_2O_3, the catalyst showed higher photocatalytic activity under visible irradiation. In particular, the release of metal ions from the catalyst was significantly inhibited during photodegradation of pollutants. Electron spin resonance and cyclic voltammograms studies under a variety of experimental conditions verified that the coupling of Au and Ag NPs increased the efficiency of light energy conversion and accelerated interfacial electron transfer processes. The main active species involved in the photoreaction of Au–Ag–AgI/Al_2O_3 were $O_2^{\bullet-}$ and excited h^+ on the metal NPs. The presence of several ubiquitous anions, including HCO_3^-, SO_4^{2-}, and NO_3^- could act as electron donors trapping excited h^+ on the metal NPs to facilitate electron circulation. The results obtained herein indicated that coupled, noble, bimetal NPs exhibited high photosensitivity and photostability due to enhanced surface plasmon resonance and interfacial electron transfer.

Keywords Visible light photocatalyst · Semiconductor-metal nanocomposites · Noble bimetal · Ion release

1 Introduction

Semiconductor-metal nanocomposites have been widely employed as photocatalysts [1–6]. In particular, nanoparticles (NPs) of noble metals can strongly absorb visible light because of plasmon resonance [7, 8], which greatly enhances the overall photocatalytic efficiency at the interface between the metal and the semiconductor. Many plasmonic photocatalysts have been developed based on this phenomenon using a combination of Ag or Au and semiconductor NPs. Several of these systems can break down various pollutants during illumination with visible light [6, 9–12]. Plasmon-induced photodegradation of pollutants is predominantly attributed to two electron transfer processes occurring simultaneously: from the photo excited noble metal NPs to the semiconductor conduction band (CB), and from a solution donor to the noble metal NPs [13, 14]. Corrosion or dissolution of the noble metal particles is inevitably involved in the photocatalytic reaction, limiting the use of noble metal Ag and Au [15]. Considerable work has gone into improving the stability of these types of photocatalysts [16–18]. Despite many promising studies, controlling the release of metal ions during photocatalytic degradation has not, to our knowledge, been reported.

It is possible that enhancing electron transfer may not only inhibit metal ion release, but also improve photocatalytic efficiency. One factor that potentially influences the electronic properties of the nanocomposite is the size of the noble metal particles. For example, Goodman and co-workers [19] have demonstrated the influence of gold NP deposition on the overall energy and catalytic activity of Titania. Size-dependent quantized conductance at metal nanocontacts has also been demonstrated [20]. In addition, the different surface potentials in multi-metal assemblies may also influence interfacial electron behavior [21].

Electronic supplementary material The online version of this article (doi:10.1007/s10562-012-0788-2) contains supplementary material, which is available to authorized users.

T. Peng · C. Hu (✉) · X. Hu · X. Zhou · J. Qu
State Key Laboratory of Environmental Aquatic Chemistry, Research Center for Eco-Environmental Sciences, Chinese Academy of Sciences, Beijing 100085, China
e-mail: huchun@rcees.ac.cn

Recently, we have shown that the plasmonic photocatalyst Ag–AgI/Al_2O_3 is highly effective in degrading toxic pollutants under visible light irradiation [13]. However, the release of Ag^+ from the catalyst was observed during the photocatalytic reaction, resulting in secondary water pollution. In this paper, in order to accelerate the cycle of electron exchange between photogenerated Ag ion and Ag NPs, which inhibit Ag^+ release, Au NPs were further loaded onto Ag–AgI/Al_2O_3 composites. The size and dispersion of noble metal—AgI NPs on mesoporous Al_2O_3 were investigated. Several ubiquitous water pollutants, including 2-chlorophenol (2-CP), phenol, and ibuprofen (IBU), were selected to investigate the plasmon effect and the charge transfer properties of the catalysts during illumination with visible light.

In a suspension of bimetallic Au–Ag–AgI/Al_2O_3, the release of Ag^+ was successfully inhibited to low levels, and no Au^{3+} was released during the degradation of pollutants due to the accelerated electron circulation. Meanwhile, the photocatalytic efficiency of the system was slightly enhanced due to increased photoabsorption. The influence of coupling between the Au and Ag NPs on light energy conversion and charge transfer was observed by electron spin resonance (ESR) studies and cyclic voltammetric (CV) analyses under a variety of experimental conditions.

2 Experimental

2.1 Materials and Reagents

5-Dimethyl-1-pyrroline-*N*-oxide (DMPO), which is used as a spin trapping agent in ESR studies, was purchased from Sigma Chemical Co. All other chemicals were analytical grade, purchased from Beijing Chemical Company, and used without further purification.

2.2 Catalyst Preparation

Mesoporous γ-Al_2O_3, AgI/Al_2O_3, and Ag–AgI/Al_2O_3 (Ag^+ content of 8 wt%) were prepared according to a previous report [13]. Au–Ag–AgI/Al_2O_3 was prepared via deposition–precipitation with urea (DPU) [22] and photocatalytic reduction methods. Briefly, 1 g of AgI/Al_2O_3 was added to 100 mL of an aqueous solution of $HAuCl_4$ (5×10^{-5} M) and urea (5×10^{-3} M). The suspension was sonicated for 1 min and vigorously stirred for 1 h at 80 °C. The product was then filtered, dried at 100 °C, and calcined in air at 500 °C for 3 h. The catalyst powder was mixed with deionized water and irradiated at 4 °C with visible light ($\lambda > 400$ nm) for 1 h to reduce Ag^+ to Ag. Finally, the product was filtered, rinsed with deionized water, and dried at ambient temperature. The prepared Au–Ag–AgI/Al_2O_3 was dark grey with an Au^0 content of 1 wt%. Following the same procedure, various amounts of Ag^+ and Au^{3+} were reduced on the AgI/Al_2O_3. As references, Au/Al_2O_3, Ag/Al_2O_3, and Au–Ag/Al_2O_3 were prepared by DPU, incipient wetness impregnation, and a combination of these two methods, respectively (see Supporting Information).

2.3 Characterization

The samples were examined by obtaining X-ray diffractograms (XDS-2000 diffractometer; Scintag Inc., Sunnyvale, CA) and UV–Vis diffuse reflectance spectra (Hitachi UV-3100). The high-resolution transmission electron microscopy (HRTEM) images associated with X-ray energy dispersive spectroscopy (EDS) analyses were performed on a JEM-2100F TEM with an acceleration voltage of 200 kV. ESR spectra were obtained using a Bruker model ESP 300 E electron paramagnetic resonance spectrometer equipped with a Quanta-Ray Nd:YAG laser system as the irradiation source ($\lambda = 532$ nm). Photocurrent from the various samples was measured in a basic electrochemical system (AMETEK Princeton Applied Research, Oak Ridge, TN) with a two-compartment, three-electrode electrochemical cell equipped with a photocatalyst photoanode (prepared by dip-coating and drying in air at 70 °C) and a platinum wire cathode in 0.1 M Na_2SO_4. The reference electrode was a saturated calomel electrode.

2.4 Photocatalytic Degradation of Pollutants Under Visible Light

Photocatalytic experiments were performed in a beaker with aqueous suspensions of pollutant (60 mL, 10 mg L^{-1}) and 100 mg of catalyst powder. The light source was a 350 W Xe-arc lamp (Shanghai Photoelectron Device Ltd.), equipped with wavelength cut-off filters for $\lambda > 420$ nm, and focused onto the beaker. Prior to irradiation, the suspensions were magnetically stirred in the dark for ca. 30 min to establish adsorption/desorption equilibrium between the pollutants and the surface of the catalyst under room air-equilibrated conditions. The concentration of each phenolic pollutant was measured using high-performance liquid chromatography (1200 series; Agilent) with an Eclipse XDB-C18 column (5 μm, 4.6 × 150 mm; Agilent). The Au^{3+} and Ag^+ concentrations were measured by inductively coupled plasma optical emission spectrometry (ICP-OES) on an OPTIMA 2000 (Perkin-Elmer Co.) instrument.

3 Results and Discussion

3.1 Characterization of Catalysts

Figure 1 shows the diffractogram obtained on various samples. Au^0 species were confirmed by four characteristic

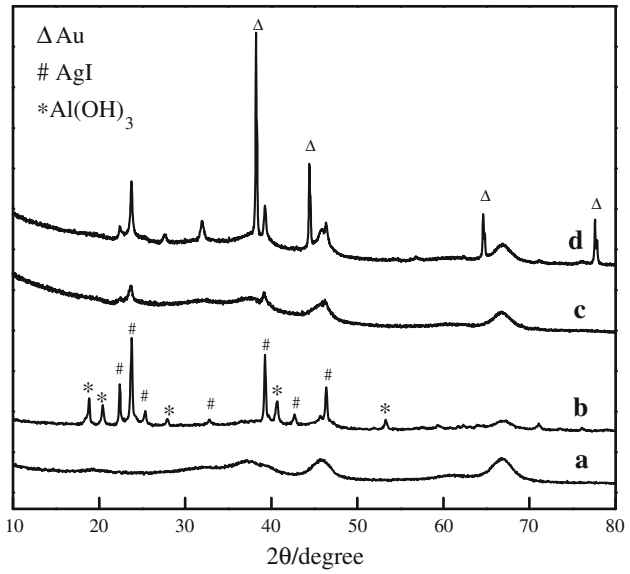

Fig. 1 X-ray diffractograms of *a* Al_2O_3, *b* AgI/Al_2O_3, *c* $Ag–AgI/Al_2O_3$, and *d* $Au–Ag–AgI/Al_2O_3$

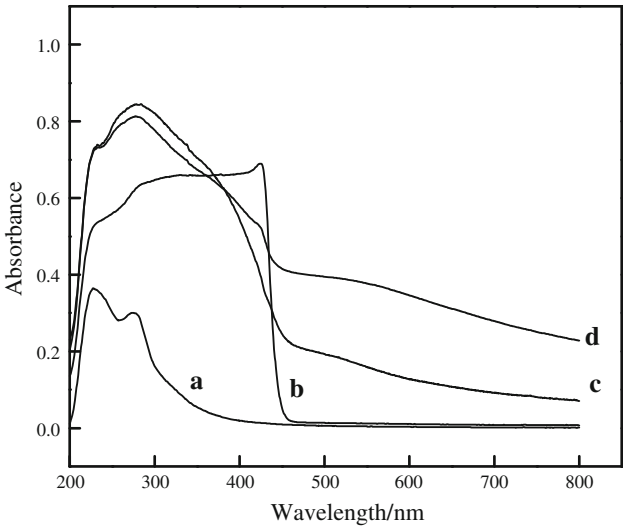

Fig. 2 Diffuse reflectance UV–Vis spectra of *a* Al_2O_3, *b* AgI/Al_2O_3, *c* $Ag–AgI/Al_2O_3$, and *d* $Au–Ag–AgI/Al_2O_3$

peaks at $2\theta = 38.2$, 44.4, 64.6, and 77.6° attributed to the (111) (200), (220), and (311) lattice planes, respectively. A mixture of β-AgI and γ-AgI was formed on AgI/Al_2O_3, $Ag–AgI/Al_2O_3$, and $Au–Ag–AgI/Al_2O_3$, while the AgI crystal size became smaller on $Ag–AgI/Al_2O_3$ and $Au–Ag–AgI/Al_2O_3$.

During catalyst preparation, the supported AgI first became amorphous after calcinations [23]. Then, the mixture of β-AgI and γ-AgI formed again on Al_2O_3 with the reduction of Ag^+ in visible-light-illuminated suspensions, leading to the observed smaller size. No diffraction peaks due to Ag^0 were observed as a result of low Ag content, small particle size, and high dispersion at the catalyst surface.

The optical properties of various samples are shown in Fig. 2. Mesoporous Al_2O_3 was transparent between 400 and 800 nm. AgI/Al_2O_3 samples exhibited a UV absorption band around 200–400 nm and a visible absorption band around 400–430 nm, which was assigned to the light absorption of AgI. $Ag–AgI/Al_2O_3$ samples exhibited a broad band in the visible region assigned to the surface plasmon absorption of Ag NPs, indicating the presence of Ag^0 on the surface. In addition, the plasmon absorption band of $Au–Ag–AgI/Al_2O_3$ became more intense and broader following the addition of Au. This phenomenon is due to an enhanced plasmon effect from intraparticle coupling in heterogeneous NPs [24].

During the preparation process, $Ag–AgI/Al_2O_3$ and $Au–Ag–AgI/Al_2O_3$ samples were photoreduced at 4 °C, while $Ag1–AgI/Al_2O_3$ was photoreduced at 30 °C. The size and dispersion of metal–AgI clusters on Al_2O_3 were characterized by HRTEM. As shown in Fig. 3, Ag–AgI and Au–Ag–AgI NPs were relatively uniform in size and highly dispersed on Al_2O_3. In contrast, the Ag–AgI NPs were aggregated on $Ag1–AgI/Al_2O_3$. Mean metal particle size was determined by TEM analysis and was based on a count of more than 300 individual NPs. Fig. 3d shows a histogram of particle size. Photoreduction at low temperature resulted in smaller particles. Coupling in the bimetallic systems resulted in narrower particle size distributions and higher dispersion on the catalyst surface.

TEM images showed that there were mainly two kinds of NPs on the surface of $Au–Ag–AgI/Al_2O_3$, spheroidal ones (Fig. 4Aa–b) and irregular ones (Fig. 4Ac), which were chosen for EDS analysis. In Fig. 4Ba–b from the spheroidal particles, the characteristic peaks were assigned to Au and Ag, respectively, suggesting that spheroidal NPs were Au or Ag, while the EDS patterns of irregular NPs showed the characteristic peaks of Ag and I in 4Bc, suggesting that irregular NPs were AgI. Characteristic peaks of Au and Ag were not observed at the same EDS spectrum in the experiment, implying that Au and Ag probably existed in form of separate spheroidal NPs rather than core–shell or alloy structures. However, Au and Ag NPs could be close or contact with each other so the surface resonance appeared through the interaction of electromagnetic fields of metal NPs [25]. Moreover, irregular NPs were observed to be contact with spheroidal NPs in Fig. 4A, which could be considered as AgI contact with Au or Ag, meaning that Au and Ag could make indirect connection with each other through AgI NPs.

3.2 Photodegradation of Pollutants Under Visible Light

To evaluate the effect of nanoparticle morphology on activity, photodegradation of 2-CP was performed in

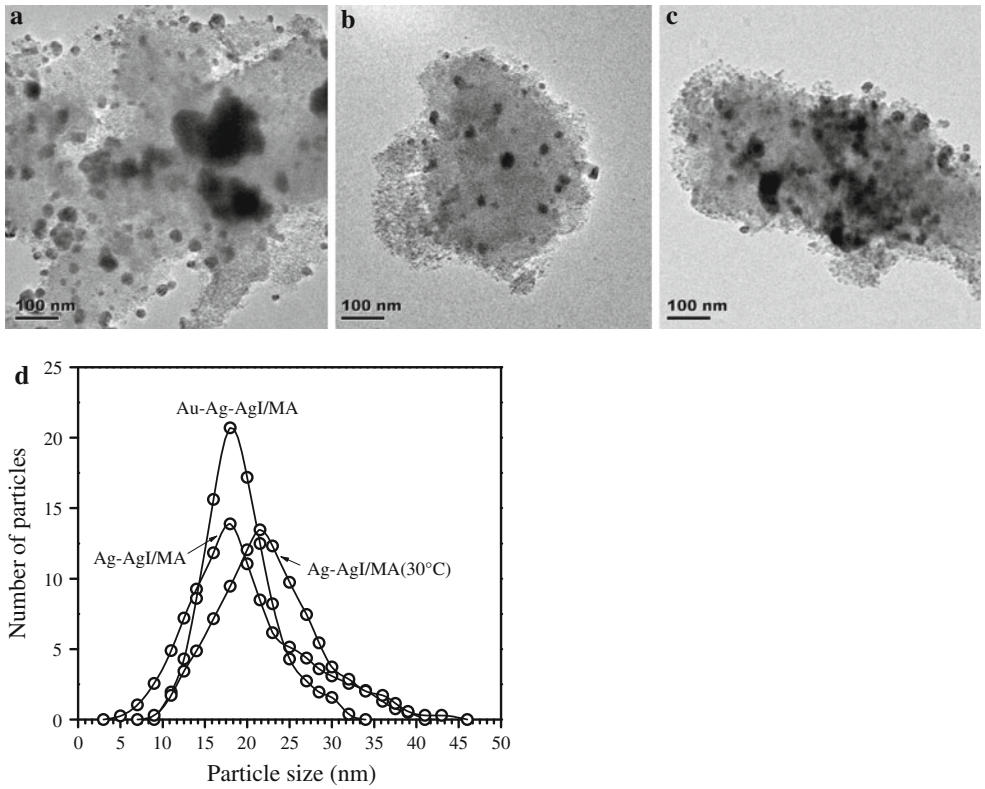

Fig. 3 Representative HRTEM images of **a** Ag–AgI/Al_2O_3, **b** Au–Ag–AgI/Al_2O_3 photoreduced at 4 °C, **c** Ag1–AgI/Al_2O_3 photoreduced at 30 °C, and **d** the particle size distribution of metal–AgI NPs on photocatalysts

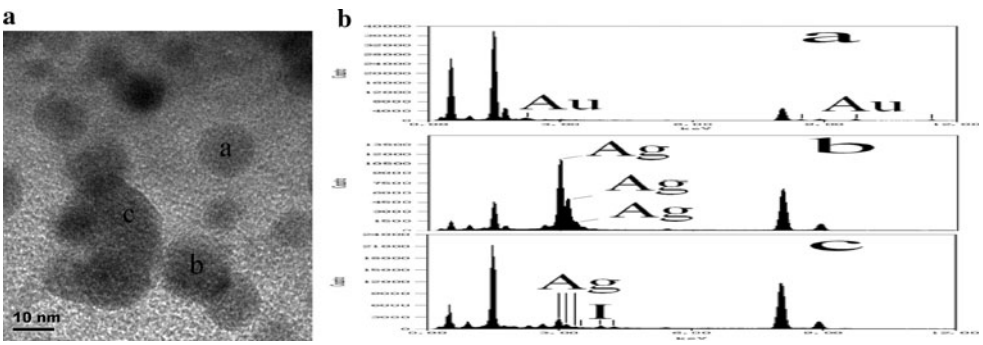

Fig. 4 **A** typical NPs of Au–Ag–AgI/Al_2O_3 chosen for EDS test, **B** EDS patterns of corresponding NPs in (**A**)

aqueous dispersions of metal–AgI NPs under visible irradiation after adsorption equilibrium (Fig. 5). 2-CP was completely degraded within 40 min by Ag–AgI/Al_2O_3 and within 30 min by Au–Ag–AgI/Al_2O_3. The activity of Ag1–AgI/Al_2O_3 was relatively poor, with 10% of the total 2-CP remaining after 40 min. The photocatalytic activity of Au–Ag–AgI/Al_2O_3 did not decrease markedly after six successive cycles of degradation testing under visible irradiation (Supporting Information Figure S1). Smaller size, a narrower particle size distribution, and a higher dispersion of metal–AgI NPs had a positive impact on the activity and stability of the photocatalyst. The results also imply an acceleration of electron transfer at the Au–Ag–AgI/Al_2O_3 surface. With the addition of Au, the interaction between Au and Ag NPs resulted in more electrons participating in a collective oscillation, thereby generating a more intense plasmon resonance. This, in turn, enhanced the efficiency of visible light utilization and photoinduced, interfacial charge transfer.

Photodegradation experiments and adsorption of IBU were also performed at various pH in order to investigate surface reactions of Au–Ag–AgI/Al_2O_3. As shown in Fig. 6, about 25% of the total IBU was adsorbed onto the catalyst. The IBU was completely photodegraded within 20 min at pH 5.6. While at pH 7.2 and 8.5, less than 20% of the IBU was adsorbed and less than 70% was

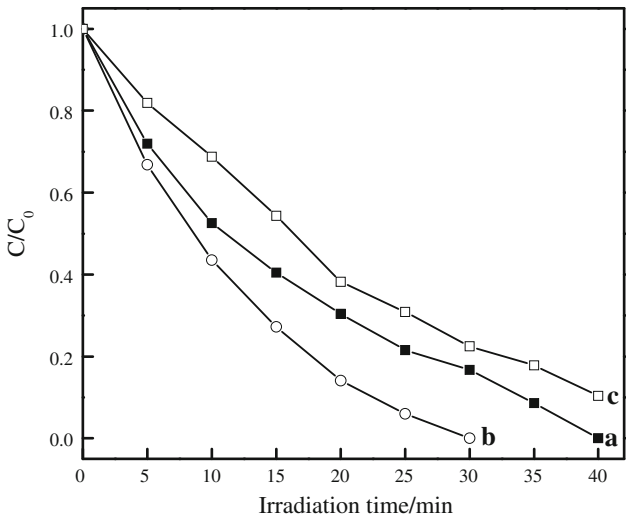

Fig. 5 The photodegradation of 2-CP (10 mg L^{-1}; 60 mL) in aqueous dispersions (containing 1.6 g L^{-1} catalyst) under visible light $\lambda > 420$ nm: *a* Ag–AgI/Al_2O_3, *b* Au–Ag–AgI/Al_2O_3, and *c* Ag1–AgI/Al_2O_3

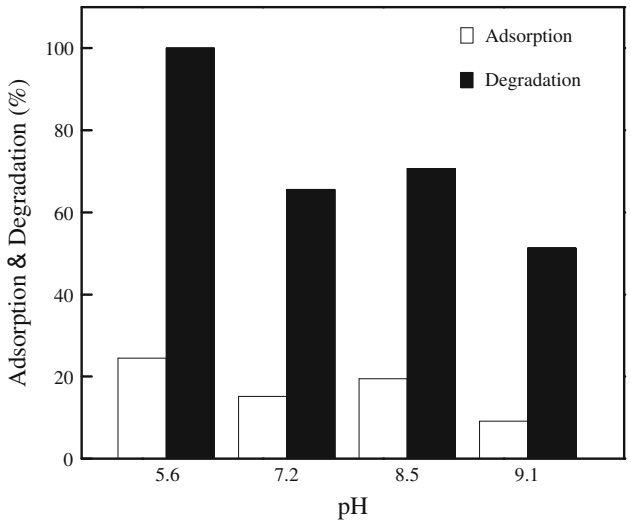

Fig. 6 The adsorption and photodegradation of IBU (10 mg L^{-1}; 60 mL) in aqueous dispersions (containing 1.6 g L^{-1} catalyst) at different pH under visible light $\lambda > 420$ nm (irradiation time: 20 min)

photodegraded after the same amount of time. At pH 9.1, the degrees of both adsorption and photodegradation were about half those at pH = 5.6. The photodegradation of IBU increased with increasing percent adsorption, indicating that surface reactions enhanced the photocatalytic efficiency of the system. In both a previous study and the current study, Au–Ag–AgI/Al_2O_3 had a similar plasmon-induced photocatalytic degradation mechanism as Ag–AgI/Al_2O_3. The interfacial reaction plays an important role in the whole photodegradation process. Since positive holes (h^+), which act as strong oxidants, are generated on Ag and Au NPs by photoexcitation, increased absorption of IBU increases the oxidation rate of h^+ and the reduction of photogenerated Ag and Au ions, thereby enhancing the photostability and photoactivity of the catalyst.

3.3 Ion Release

Figure 7 shows the release of Ag^+ and Au^{3+} during the photodegradation of 2-CP. The amount of Ag^+ released decreased slowly as the reaction proceeded in both Ag–AgI/Al_2O_3 and Au–Ag–AgI/Al_2O_3 suspensions. At the point of complete degradation, the final concentration of Ag^+ was 0.17 ppm in Au–Ag–AgI/Al_2O_3, approximately three times less than the 0.55 ppm concentration observed in the Ag–AgI/Al_2O_3 suspension. No trace of Au^{3+} was found in the Au–Ag–AgI/Al_2O_3 suspension throughout the entire reaction. The redox potential of Au^{3+} indicates a higher oxidation activity than Ag^+. Therefore, the gold was more easily reduced by 2-CP, which would inhibit the release of gold ion.

Chloride ion, a degradation product of 2-CP, potentially interfered with measurements by combining with Ag^+. To avoid this, phenol was used as a photodegradation substrate to investigate metal release and charge transfer reactions. The results in Fig. 8 are similar to those obtained with 2-CP. About 90 and 80% of phenol were degraded within 60 min in Au–Ag–AgI/Al_2O_3 and Ag–AgI/Al_2O_3 suspensions, respectively. Correspondingly, the amounts of Ag^+ released were 4 and 8 ppm with no Au^{3+} ion detected. The higher photocatalytic efficiency, and lower amounts of metal released, confirmed that the coupling of Au and Ag NPs enhanced the efficiency of interfacial charge transfer

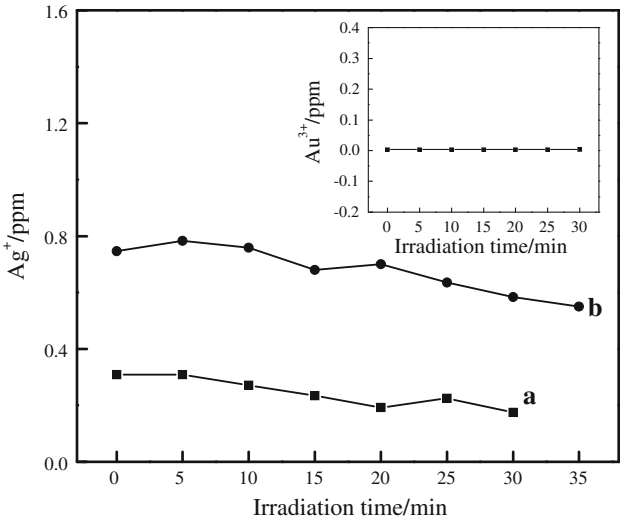

Fig. 7 Ag^+ release during the photodegradation of 2-CP (10 mg L^{-1}) in aqueous dispersions of catalyst under visible light $\lambda > 420$ nm: *a* Au–Ag–AgI/Al_2O_3 and *b* Ag–AgI/Al_2O_3. The inset shows Au^{3+} release from Au–Ag–AgI/Al_2O_3

processes. This, in turn, indicated that the release of metal ions was related to electron transfer.

Therefore, the release of both Ag and Au ions was examined in various NP suspensions. As shown in Fig. 9, almost no dissolved metal ions were observed in Ag/Al_2O_3, Au/Al_2O_3, or $Au–Ag/Al_2O_3$ suspensions in the absence of light. When irradiated with visible light, however, some Ag^+ appeared in the Ag/Al_2O_3 suspension, but no Au^{3+} was observed in the Au/Al_2O_3 suspension. This indicates that less photoinduced electron transfer occurred in the monometallic NPs. In contrast, both Ag^+ and Au^{3+} were released in relatively large quantities from photoexcited $Au–Ag/Al_2O_3$. This indicates coupling between Au and Ag and an enhancement in interfacial electron transfer. In addition, with AgI acting as an electron acceptor, charge recombination was suppressed and electron–hole separation was accelerated, leading to higher levels of Ag^+ in photocatalyst suspensions containing AgI. These results confirm that the addition of Au accelerated electron transfer and suppressed the release of Ag^+ and Au^{3+} ions in $Au–Ag–AgI/Al_2O_3$ suspensions under visible light.

Several common inorganic anions were also added to the reaction system in order to determine their effect(s) on charge transfer. Under otherwise identical conditions, the addition of anions suppressed the release of Ag^+. The effect was especially potent in tap water, which contained a high variety of anions, although the efficiency of the catalytic system was decreased (Fig. 10). HCO_3^-, SO_4^{2-}, and NO_3^- can be adsorbed onto the surface of the catalyst. The adsorbed inorganic anions then react with photoinduced Ag^+ (electron holes h^+) and adsorbed $^\bullet OH$ to form $HCO_3^\bullet$, $SO_4^{\bullet-}$, and $NO_3^\bullet$, which are less reactive than h^+ and $^\bullet OH$ [26]. The lower the amount of Ag^+ released, the more likely it was that Ag^+ would obtain electrons from anions reverting to their initial state. This results in an overall increase in charge circulation.

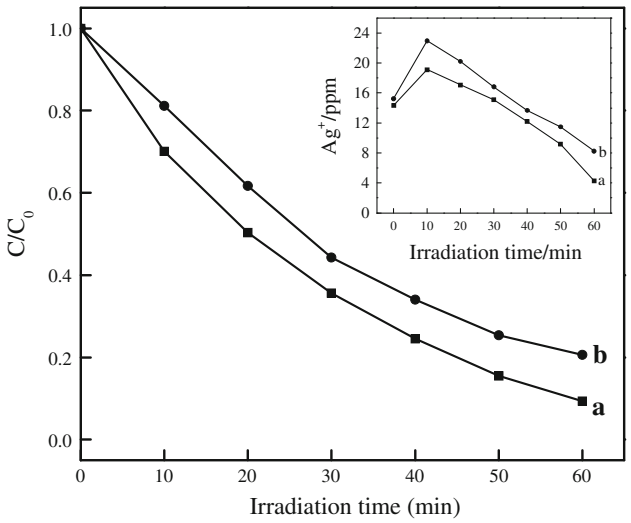

Fig. 8 Photodegradation of phenol (10 mg L^{-1}; 60 mL) in aqueous dispersions (containing 1.6 g L^{-1} catalyst) under visible light $\lambda > 420$ nm: *a* $Au–Ag–AgI/Al_2O_3$ and *b* $Ag–AgI/Al_2O_3$. The *inset* shows the release of Ag^+

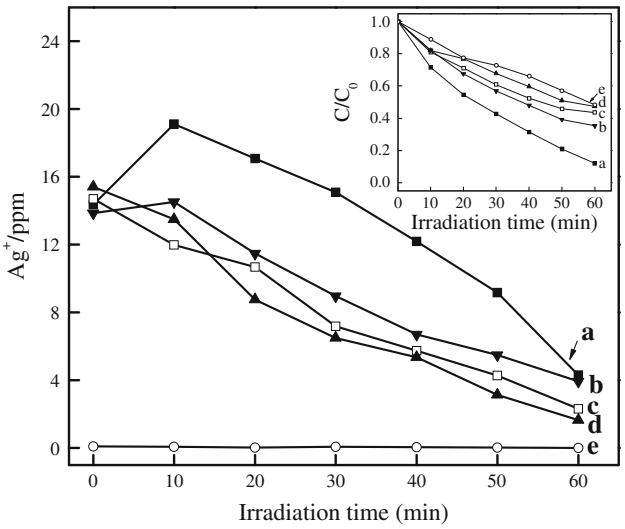

Fig. 10 Ag^+ release during the photodegradation of phenol (10 mg L^{-1}) in $Au–Ag–AgI/Al_2O_3$ suspension (1.6 g L^{-1}) under visible irradiation ($\lambda > 420$ nm) with the addition of anions: *a* catalyst only, *b* $NaHCO_3$, *c* Na_2SO_4, *d* $NaNO_3$, and *e* phenol in tap water with catalyst. Anion concentration: 0.1 M. The *inset* shows the temporal course of corresponding photocatalytic reactions

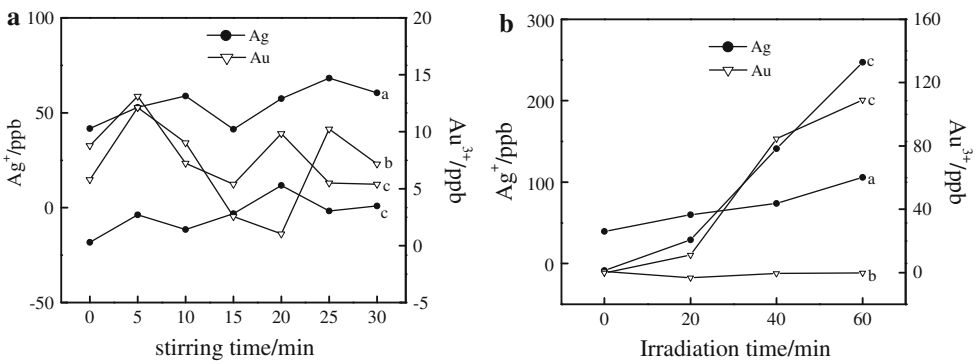

Fig. 9 Ions released from different catalysts in water: **A** in dark and **B** under visible light $\lambda > 420$ nm. For all panels, *a* Ag/Al_2O_3, *b* Au/Al_2O_3, and *c* $Au–Ag/Al_2O_3$

3.4 Plasmon-Induced Interfacial Charge Transfer in Au–Ag–AgI/Al_2O_3

The reduction potential of the CB of AgI is −0.15 V. Therefore, an electron in the CB of plasmon-induced metal NPs can reduce oxygen to $O_2^{\bullet-}$ [27]. ESR studies were performed with DMPO to determine $O_2^{\bullet-}$ levels and elucidate interfacial electron transfer in photocatalyst suspensions (Fig. 11). Signals corresponding to DMPO-$O_2^{\bullet-}$ were detected in the Au–Ag–AgI/Al_2O_3 suspension even under weak indoor lighting. These same signals were not observed in the Ag–AgI/Al_2O_3 suspension even under identical conditions. With visible light irradiation (532 nm), both systems generated $O_2^{\bullet-}$. These results verified that bimetallic Au–Ag NPs enhanced the electron transfer from metal NPs to the CB of AgI, even with extremely weak photoexcitation.

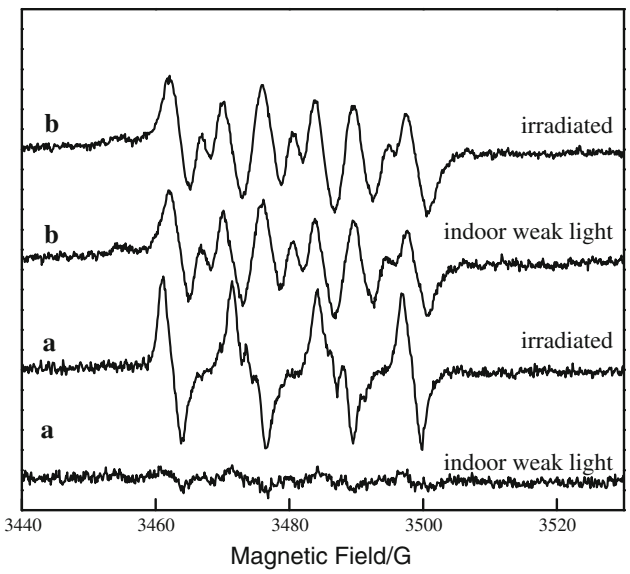

Fig. 11 The ESR signal of the DMPO-$O_2^{\bullet-}$ in various methanol dispersions before and after irradiation with visible light (532 nm): *a* Ag–AgI/Al_2O_3 and *b* Au–Ag–AgI/Al_2O_3

The transfer characteristics of enhanced, plasmon-induced charges were also determined by cyclic voltammetry (CV). In an aqueous, nitrogen-saturated 0.1 M solution of sodium sulfate under visible irradiation (Fig. 12A), the photocurrent increased and then decreased to zero, resulting in a peak attributed to the oxidation of metal NPs. With the incorporation of Au NPs, the intensity of this peak increased due to enhanced plasmon resonance, charge separation, and transfer. Due to its poor absorption of visible irradiation ($\lambda > 420$ nm), only a weak photocurrent (approximately zero) was detected at the AgI/Al_2O_3 photoanode. A similar phenomenon was observed in an aqueous, air-saturated 0.1 M sodium sulfate solution, although photocurrent differences became much more significant (Fig. 12B). In the presence of air, O_2 in the water acted as an electron acceptor and trapped the CB electrons of AgI from plasmon-induced metal NPs to form $O_2^{\bullet-}$, which served to promote electron transfer. The photocurrent differences of these three catalysts coincided with their respective photocatalytic activities.

Neither the Au nor Ag NPs showed any obvious signs of oxidation on Al_2O_3 in N_2 or air, even under illumination with visible light. When combined, the Au and Ag NPs produced a relatively intense oxidation peak under identical conditions. These results distinctly reflect an increase in light energy conversion by bimetallic coupling (Supporting Information Fig. S2). Figure 13 shows the effects of different electron donors on the photocurrent in aqueous, air-saturated solutions of 0.1 M sodium sulfate. With the addition of 2-CP, the peak gradually decreased and became indiscernible at 100 ppm (Fig. 13a). This indicates that plasmon-induced holes on metal NPs were capable of trapping electrons from pollutants. As shown in Fig. 13b, c, the peak also gradually decreased to indiscernible levels with the addition of HCO_3^- or NO_3^-. These results confirm that the above anions were

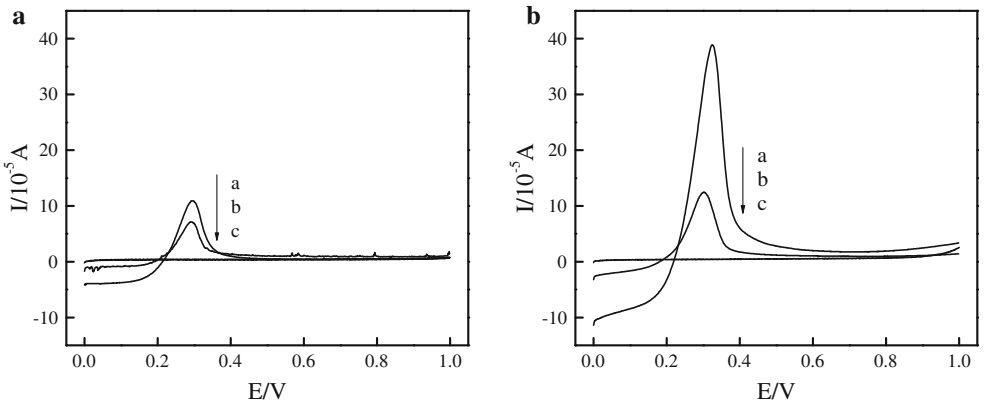

Fig. 12 Changes in photocurrent are shown at different photoanodes under visible irradiation ($\lambda > 420$ nm) in **A** N_2-saturated and **B** air-saturated solutions of 0.1 M aqueous sodium sulfate: *a* Au–Ag–AgI/Al_2O_3, *b* Ag–AgI/Al_2O_3, and *c* AgI/Al_2O_3

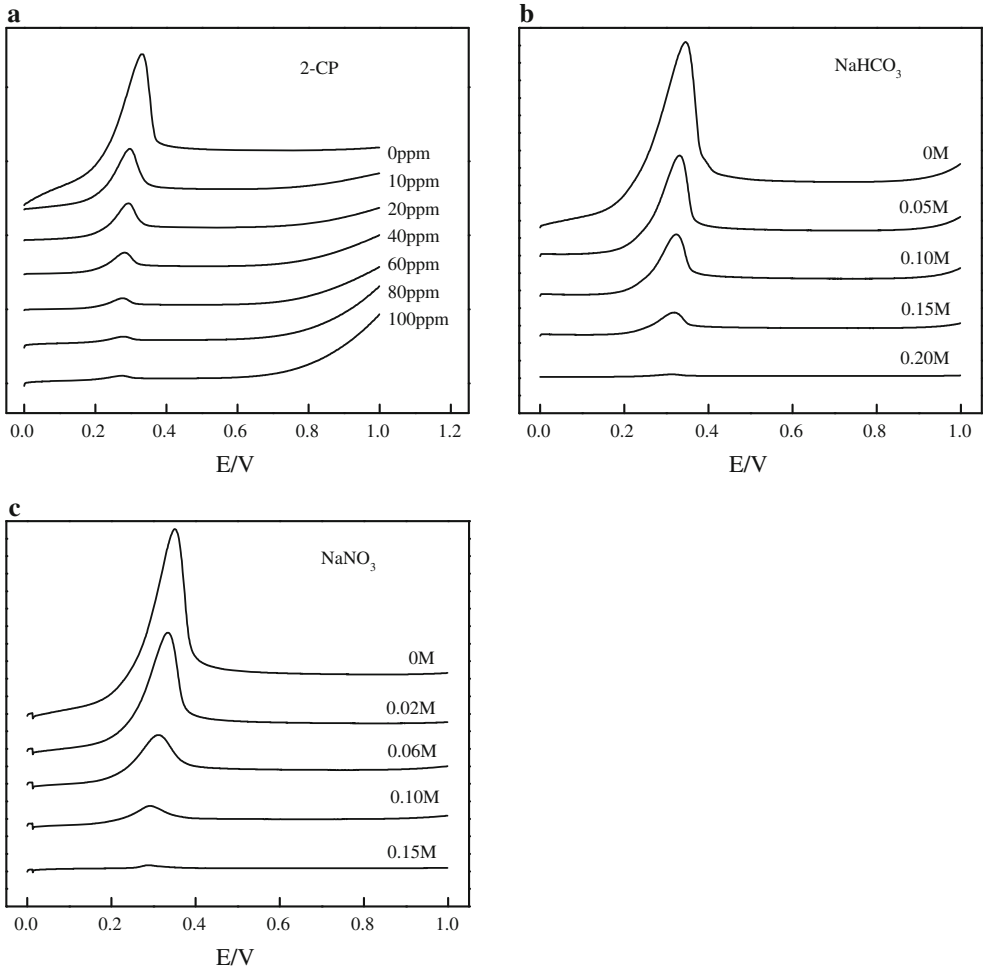

Fig. 13 The effects of various electron donors on the photocurrent at the Au–Ag–AgI/Al_2O_3 photoanode are shown under visible irradiation ($\lambda > 420$ nm) in aqueous, air-saturated 0.1 M sodium sulfate

able to donate electrons to photoexcited holes forming $HCO_3^{\bullet}$ or $NO_3^{\bullet}$ radicals, thereby enhancing electron transfer and suppressing the release of Ag^+. The overall effect, however, was a reduction in catalytic activity because the anion radicals were less reactive than h^+.

4 Conclusions

Au–Ag–AgI were deposited uniformly and were well dispersed on mesoporous alumina substrates by deposition–precipitation and photoreduction at low temperature. Coupling of bimetallic NPs not only narrowed the Au–Ag–AgI particle size distribution and increased the particle dispersion on Al_2O_3, but also increased plasmon resonance. The coupled catalysts showed higher photocatalytic activities under visible irradiation. In particular, the release of metal ions from the catalyst was significantly inhibited during the photodegradation of pollutants. Furthermore, studies of ESR and CV measurements under a variety of experimental conditions verified that coupling of Au and Ag NPs increased light energy conversion and accelerated interfacial electron transfer processes. It was found that several ubiquitous anions, including HCO_3^-, SO_4^{2-}, and NO_3^-, acted as electron donors and trapped excited h^+ on metal NPs thereby increasing electron circulation. All of the above results demonstrated that coupled noble bimetal NPs can be extremely photosensitive and photostable due to enhanced surface plasmon resonance and interfacial electron transfer.

Acknowledgments This study was supported by the 973 project (No. 2010CB933604), the NSFC (Nos. 20807051, 50921064) and the Federal Department of Chinese Water Control and Treatment (No. 2008ZX07209-001).

References

1. Henglein A (1989) Chem Rev 89:1861–1873
2. Haruta M (1997) Catal Today 36:153–166

3. Valden M, Lai X, Goodman DW (1998) Science 281:1647–1650
4. George Thomas K, Kamat PV (2003) Acc Chem Res 36:888–898
5. Subramanian V, Wolf EE, Kamat PV (2004) J Am Chem Soc 126:4943–4950
6. Awazu K, Fujimaki M, Rockstuhl C, Tominaga J, Murakami H, Ohki Y, Yoshida N, Watanabe T (2008) J Am Chem Soc 130:1676–1680
7. Jin R, Cao YC, Mirkin CA, Kelly KL, Schatzand GC, Zheng JG (2001) Science 294:1901–1903
8. Link S, El-Sayed MA (1999) J Phys Chem B 103:8410–8426
9. Hu C, Lan Y, Qu J, Hu X, Wang A (2006) J Phys Chem B 110:4066–4072
10. Georgekutty R, Seery MK, Pillai SC (2008) J Phys Chem C 112:13563–13570
11. Wang P, Huang B, Qin X, Zhang X, Dai Y, Wei J, Whangbo M (2008) Angew Chem Int Ed 47:7931–7933
12. Wang P, Huang B, Qin X, Zhang X, Dai Y, Whangbo M (2009) Inorg Chem 48:10697–10702
13. Hu C, Peng TW, Hu XX, Nie YL, Zhou XF, Qu JH, He H (2010) J Am Chem Soc 132:857–862
14. Tian Y, Tatsuma T (2005) J Am Chem Soc 127:7632–7637
15. Subramanian V, Wolf EE, Kamat PV (2003) Langmuir 19: 469–474
16. Dick K, Dhanasekaran T, Zhang Z, Meisel D (2002) J Am Chem Soc 124:2312–2617
17. Elahifard MR, Rahimnejad S, Haghighi S, Gholami MR (2007) J Am Chem Soc 129:9552–9553
18. Sangeetha P, Zhao B, Chen Y-W (2010) Ind Eng Chem Res 49:2096–2102
19. Yang ZX, Wu RQ, Goodman DW (2000) Phys Rev B 61: 14066–14071
20. Li J, Yamada Y, Murakoshi K, Nakatoa Y (2001) Chem Commun 2170–2171
21. Kalsin AM, Fialkowski M, Paszewski M, Smoukov SK, Bishop KJM, Grzybowski BA (2006) Science 312:420–424
22. Zanella R, Giorgio S, Henry CR, Louis CJ (2002) Phys Chem B 106:7634–7642
23. Uvarov NF, Bokhonov BB, Politov AA, Vaněk P, Petzelt J (2000) J Mater Synth Process 8:327–332
24. Shibata T, Bunker BA, Zhang Z, Meisel D, II Vardeman CF, Gezelter JD (2002) J Am Chem Soc 124:11989–11996
25. Kim S, Kim SK, Park S (2009) J Am Chem Soc 131:8380–8381
26. Ross AB, Neta P (1979) U.S. Department of Commerce, National Bureau of Standards, Washington, DC
27. Li Y, Zhang H, Guo Z, Han J, Zhao X, Zhao Q, Kim S (2008) Langmuir 24:8351–8357